

Geothermal Exploration Through Deep Exploratory Slimholes: Singapore's Perspective

Alessandro ROMAGNOLI¹, Jonathan POH¹, Tobias MASSIER², Hendrik TJIAWI^{1,3}, Wei WU¹, Anurag CHIDIRE^{4,2},
Dazhao LU¹, Jerry CHAN¹, Lizhong YANG¹, Jian Wei Mark LIM¹, Cliff Khiok Eng CHUA³

¹Nanyang Technological University, ²TUMCREATE, ³Surbana Jurong, ⁴Technical University of Munich,

a.romagnoli@ntu.edu.sg

Keywords: Geothermal, Slimhole exploration, Geology, Techno-environmental analysis, Urban environment

ABSTRACT

Singapore is a small, densely populated urbanized city-state that relies on energy imports for self-sustainability and security due to the lack of natural resources. Aside from renewable energy sources, including solar energy, geothermal power could also be a viable domestic source of energy. Hot springs and anomalous regional heat flow indicate that the country have geothermal potential. Two deep exploratory slimholes have been conducted in northern Singapore to ascertain the presence of this resource.

The first slimhole, located at Admiralty, reached a depth of about 1.16 km in February 2023, while the second slimhole at Sembawang reached a depth of 1.76 km in February 2024. The evaluated geothermal gradient at these sites exceeds the global average for continental regions, with temperatures at depths surpassing those in many other non-volcanic areas worldwide. Heat production from the granites is found to be higher than average compared to other granites worldwide. Extrapolated temperature data to depths of 4 – 5 km is high enough for various applications, including “green” electricity generation, hydrogen production, district cooling, and desalination.

Geothermal heat extraction for electricity generation and space cooling are also considered. Techno-environmental results indicate that utilizing geothermal resources will significantly reduce carbon emissions even though most of the country's electricity is generated by burning natural gas, the cleanest fossil fuel. Considering that one-third of the electricity generated is used for cooling, the potential to meet a portion of this demand with geothermal energy would significantly enhance the country's ongoing decarbonization initiatives. Moreover, the leveled cost of electricity is found to be competitive with other renewable energy sources.

In conclusion, the results are in favor for Singapore's geothermal potential, warranting further exploration to depths of around 5 km. Utilization cases demonstrate their potential contribution to Singapore's decarbonization efforts, making geothermal energy initiatives significant for sustainable energy development.

1. INTRODUCTION

Energy security is a critical concern for any country, as it ensures the stable and reliable supply of energy necessary for economic growth, national security, and the well-being of its citizens. The past few years have highlighted the importance of energy security, with the volatility of energy prices reaching unprecedented levels due to global instability. Events such as the COVID-19 pandemic and the ongoing Russia-Ukraine war have disrupted supply chains and caused significant fluctuations in energy markets (up to 70% increase, Zhang et al. (2024)), underscoring the need for countries to secure their energy sources. In response to these challenges, many countries, especially in the European Union, have increased their investments in domestic energy production, especially in renewable energy sources such as wind, solar, and geothermal (IEA 2024).

Despite being a small city-state, Singapore has a high population density and relies heavily on imports to maintain urban self-sustainability and energy security, given its lack of known natural resources for extraction and use. Most of Singapore's energy supply is from imported natural gas. The city-state has been exploring various clean energy options to diversify its portfolio, including hydrogen-ammonia and solar photovoltaic while reducing carbon emissions. Solar, for instance, is one of the cheapest clean energy technologies to deploy (e.g., Lazard 2024), but the high surface footprint requirement makes it challenging for land-scarce countries like Singapore to install high capacities. A new source is needed, one that must be capable of providing a clean baseload generation independent of environmental conditions. Geothermal energy has emerged as the prime candidate for implementation should a significant heat source be discovered, motivating the purpose of this work. Furthermore, the government has already considered geothermal power to be part of its future energy portfolio by 2050 (EMA 2022).

The National Research Foundation awarded a grant to a team from Nanyang Technological University (NTU) and TUMCREATE, partnering with Surbana Jurong, to investigate the feasibility of geothermal energy in Singapore. In northern Singapore, two deep exploratory slimholes were drilled to measure subsurface temperatures and retrieve rock cores. These cores offer a valuable chance to explore Singapore's deep geological framework and create essential datasets. This work presents the groundbreaking study of Singapore's geothermal potential, highlighting the results obtained from the recent drillings.

The structure of this paper is as follows. We start with an overview of the geological and geothermal features of Singapore. The next section describes the methodology on the processes employed during site selection, laboratory analyses and temperature measurements. Drilling of the exploratory slimholes obtained data, and the results of their analysis are described for the first time with a focus on the

subsurface rock conditions, analysis of laboratory measurements, and their respective measured temperature profiles. The paper concludes with the discussion on the geothermal potential, possible utilization cases from techno-economic analyses, and the significance and limitations of the work.

2. GEOLOGICAL AND GEOTHERMAL FEATURES OF SINGAPORE

In Figure 1, the general geology of Singapore is divided into the following blocks: variegated arc-derived granites and dykes at the center and towards the east (Gillespie et al. 2019), very-low metamorphic grade sedimentary rocks with pyroclastic-tuff related rocks towards the east and offshore islands (Dodd et al. 2019; 2020), and a series of marine and terrestrial sedimentary rocks to the west (Chua et al. 2020). The near-surface geological features are well understood up to the first few hundred meters, partly due to the abundance of shallow boreholes and building works (Leslie et al. 2019).

Among the arc-derived granites, the Simpang granite is of particular interest for its elevated concentrations of heat-producing elements (i.e., Uranium, Thorium and Potassium) in these granites lead to heat production values of $7 - 8 \mu\text{W/m}^3$, which is more than double the global averaged granite heat production (Bea 2012). The loci of the Simpang granite are currently understood to be extensive by being the basement rock for about one-third of the country. The Simpang granite has the following defining features according to Gillespie et al. (2019). Firstly, the Simpang granite is identified as the youngest of the arc-derived granites (at U/Pb age of ~ 230 Myr). Secondly, the granite has a higher proportion of felsic minerals such as feldspars and plagioclases due to its $>70\%$ Si content, thus classifying the granite as a syenogranite. Lastly, the granite can be formed via the mingling of felsic and mafic magmas that results in a localized banded layering of dark and light-colored rock types, providing a useful field description during the rock core extraction process.

The city-state has several naturally occurring hot springs, of which the Sembawang hot spring is the most studied, and it resides within the Simpang granite pluton. The Sembawang hot spring was first studied to determine its hydrogeological features (Zhao, Chen, and Cai 2002). The current hypothesis suggests that the Sembawang hot spring is part of a hydrothermal system where meteoric water percolates to depths of 5 km, gets heated and flows upwards due to thermal buoyancy through a complex network of fractures and cracks to form hot springs on the surface. Surface temperatures of the Sembawang hot spring are at least 70°C . Previous Na/K geothermometer analysis indicates a mean reservoir temperature of 163°C (Santoyo and Diaz-González 2010). The estimated reservoir temperatures are favorable to generate electricity that can substantiate baseload power generation (Oliver et al. 2011). Numerical simulations indicate that subsurface temperatures of $125 - 150^\circ\text{C}$ can be found at depths of $1.25 - 2.75$ km beneath the Sembawang hot springs (Tjiawi, Palmer, and Oliver 2012).

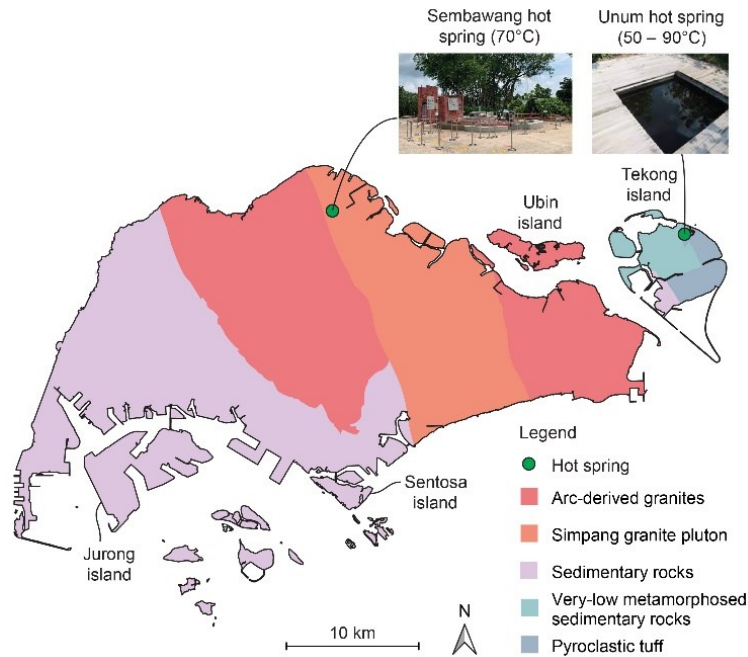


Figure 1: Simplified geological map of Singapore with the locations of the Sembawang and Tekong Island hot springs adapted from Gillespie et al. (2019) and Building and Construction Authority (2021).

Global heat flow maps show elevated heat flows exceeding 60 mW/m^2 along major tectonic boundaries, particularly towards the west of the northern and southern American continents and Southeast Asia (dashed box in Figure 2A). A reconstruction of the heat flow data by Hall and Morley (2004) indicate anomalous heat flows in Singapore ranging from 110 mW/m^2 in the East to 130 mW/m^2 in the West of the island (in Figure 2B). The cause for the anomaly could be attributed to nearby subduction-related arc magmatism and extensional deformation in Sumatra and Java (Siringoringo et al. 2024). The high heat flows suggest that Singapore could have geothermal potential at relatively shallow depths. Additionally, the hot springs in Singapore are part of the southeastern trajectory of regional hot springs located along Peninsula Malaysia, further reinforcing the presence of a regional thermal system (Baioumy et al. 2015; Oliver et al. 2011).

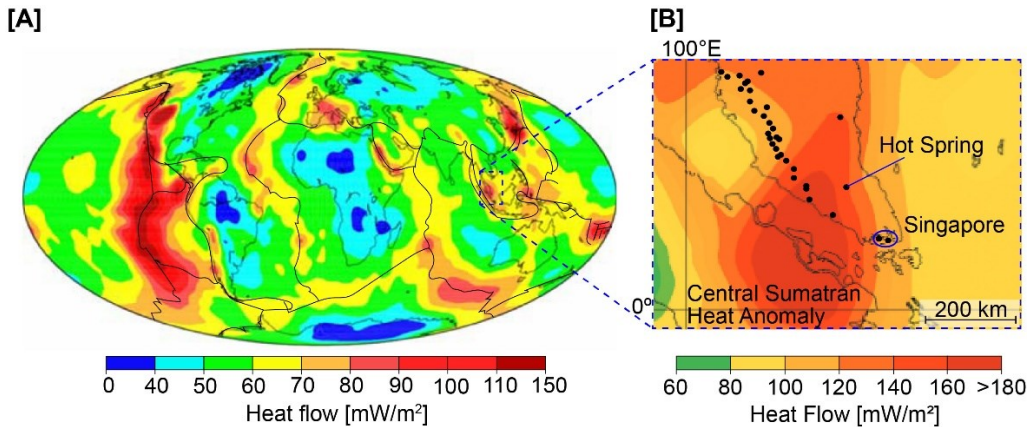


Figure 2: [A] Global heat flow map with tectonic plate boundaries as solid black lines. Dashed line box highlights [B] the regional heat flow map around Singapore and the Central Sumatra heat anomaly with hot springs. Modified from Hamza, Cardoso, and Ponte Neto (2008) and Hall and Morley (2004). Hot spring locations superimposed in [B] are from (Baioumy et al. 2015).

3. METHODOLOGY

3.1 Site selection process

In Figure 3, temperature data from existing boreholes reaching depths up to 300 m were used to develop a near-surface temperature distribution map. The map indicates that the hotter region is in northern Singapore, around the Sembawang hot spring, which we decided to focus our exploration on. Other considerations for the site selection are site accessibility, whether the site has sufficient space buffer from other buildings, and whether the site is available for use for the duration of our study. Two sites were selected out of the possible locations: one at Admiralty Lane and another at Sembawang, which are approximately 0.6 km and 2.7 km away from the Sembawang hot spring, respectively.

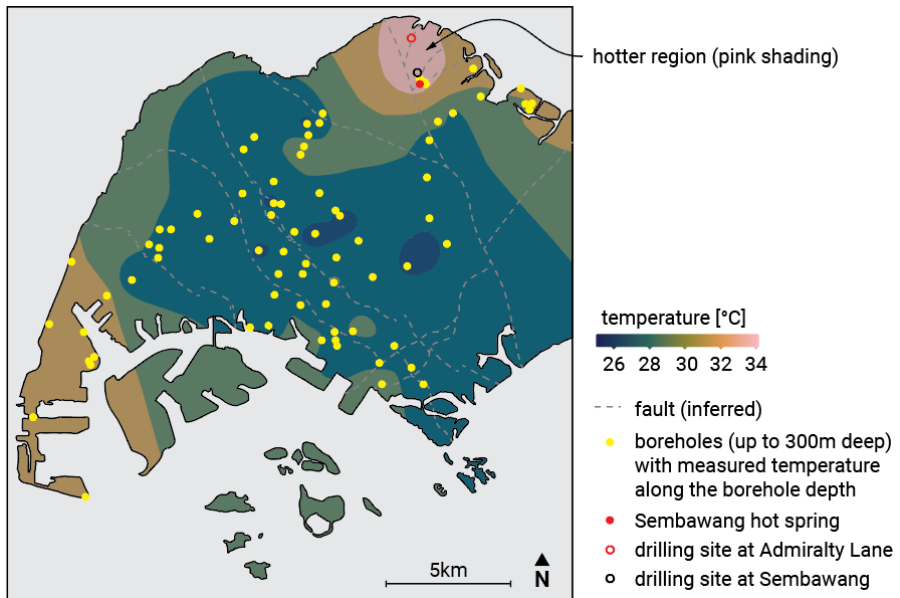


Figure 3: Near-surface temperature distribution map of Singapore based on data from shallow boreholes (up to 300m deep). The hotter region is found within the pink region in northern Singapore, near the Sembawang hot spring. The figure is modified from a map created by using Sequent Leapfrog Energy.

3.2 Laboratory measurements (rock core designation, rock core density, thermal conductivity and heat production)

Geotechnical logging was performed throughout the drilling and rock core extraction process, generating datasets such as the rock quality designation (RQD). RQD is defined as the sum length of all core pieces with at least one full diameter that is 100 mm or longer between natural fractures, measured along the center line of the core, and is expressed as a percentage of the length of the core length (e.g., Annels and Dominy 2003). RQD values also provide a quantitative approximation to the integrity of the rocks at depth and identify weak zones.

200 rock core samples from both slimholes have been selected systematically at every 15 meters for rock core density, thermal conductivity and X-ray fluorescence (XRF) measurements. The selected rock core samples are first cut using a Buehler 10-inch trim saw into 5 – 10 cm lengths (in Figure 4A). The rock cores from Admiralty and Sembawang sites are often found with pre-existing fractures and lines of weakness. Rock samples that remain intact after cutting are then used for thermal conductivity and density measurements using the C-Therm Modified Transient Plane Source sensor (in Figure 4B), which was chosen for its measuring speed and compatibility with various sample sizes. Rock core densities were obtained from the measured weight, diameter, and core heights (in Figure 4C).

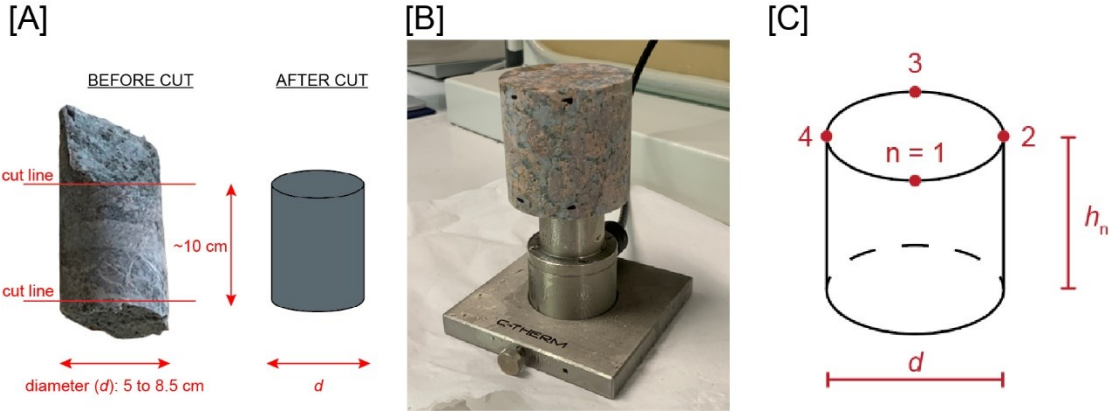


Figure 4: [A] Preparation of rock core for thermal conductivity measurements, [B] thermal conductivity measurement of the rock core with the C-Therm Modified Transient Plane Source sensor, and [C] points of measurements of the rock core when evaluating its density. d and h_n are diameter and height of rock core at each point, respectively.

After preparing the rock samples for thermal conductivity analysis, the balance of the rock core is cut, dried and crushed using the 2894 Fritsch Jaw Crusher and the 1241 Fritsch Cup Miller, and then air-dried for at least 48 hours. XRF measurements are taken using the Bruker Tiger S8 after preparing sample pellets with a 10:1 ratio of rock sample to Boreox binding agent.

Despite best efforts to select rock core samples with less observable lines of weaknesses, the cementing within the rock's pre-existing fractures would fail during the sample preparation, rendering the sample useless for rock density and thermal conductivity measurements. Thus, many samples were taken to overcome this limitation. The number of measurements taken for XRF and thermal conductivity for both slim holes are 165 and 162, respectively.

Calibration curves for U, Th and K₂O were generated using reference samples (NCS DC sample 73302, 73301, 73304 and 73305; JG-1, JG-3, CGL-008, JG-1a). These reference samples were selected based on the granite rock type comparable to the Simpang Granite. In Table 5, the standard deviation and squared correlation coefficient values for each element are at least 0.97. The applied measurement method is customized to perform long scans around the corresponding U, Th, and K₂O K_{α1} values of 98439, 93350 and 3314 eV, respectively. The voltage and current applied to the LiF200 and PET crystals are 30 – 60 kW and 81 – 135 mA, respectively. As these calibration curves will result with accurate U, Th and K₂O measurements, the statistical accuracy for measuring other elements and oxides, such as TiO₂, Na₂O, B, Be, Bo and Ti, will not be optimal.

Table 5: Applied calibration curves to XRF measurements for K₂O, U, and Th.

Element	Range	Standard deviation	Squared correlation coefficient
K ₂ O	0.65 – 5.01 wt%	0.26 wt%	0.97
U	3 – 54 ppm	1 ppm	1.00
Th	2 – 19 ppm	0.60 ppm	1.00

After acquiring the elemental concentrations from the rock samples, radiogenic heat production, A , is then calculated based on the equation from Bücker and Rybach (1996) which is expressed as:

$$A = 10^{-5} \times \rho_r \times (9.52 C_u + 2.56 C_{Th} + 3.48 C_{K2O}) \quad (1)$$

where ρ_r , C_u , C_{Th} , C_{K2O} are rock density (kg/m³), and concentrations of U (PPM), Th (PPM) and K₂O (wt %).

3.3 Downhole temperature measurements and heat flow

Downhole temperatures are measured after they have been allowed to reach equilibrium with the surrounding rock temperatures. As such, the slimholes are to be left undisturbed for an extended duration after drilling has stopped. However, the length of time (i.e., stabilization

time) required is not clearly defined (e.g., a few hundred days as in Satman and Tureyen 2016). Given the time constraints and the running costs, a lengthy stabilization time is not feasible. A 12-hour stabilization time has been proposed as a guideline, considering that slimhole temperatures reach equilibrium much faster than production-sized boreholes. We have also advised the drilling team to allow a longer stabilization time if their schedule allows. For instance, temperature measurements can occur during machinery and site maintenance periods and after extended public holidays lasting at least 72 hours. Stabilized temperatures were observed in consecutive measurements.

Temperature measurements were taken using the Hobo U12-015-03 Data Logger fastened onto the drilling wire and encased in a metal housing (Figure 6A). Temperatures were measured in two directions: top to bottom and bottom to top of the slimhole. The average speed of the lowering/raising of the temperature probe in the well was timed around 15 cm/s. The drilling wires were pre-marked with yellow tape to maintain consistency in the distance intervals (in Figure 6B). Multiple readings were taken, and the temperature profiles presented in this paper are the finalized versions.

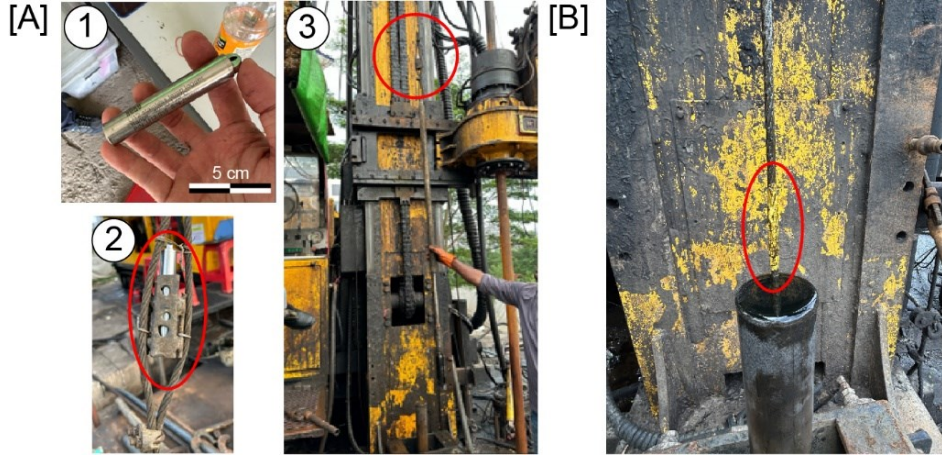


Figure 6: [A] Setting up of the (1) Hobo U12-015-03 temperature data logger, (2) metal housing for the temperature probe, and (3) the placement of the data logger onto the drilling wire (3). [B] yellow markings on the drilling wire at intervals of 25 m.

Once the temperature readings were acquired, the temperature profiles were evaluated, and the following guiding assumptions were made: a linear least-squared approach of the points and the regression value to be at least 0.95.

Subsequently, heat flow can be computed using Fourier's law of thermal conduction, which is expressed as:

$$q = -k_r \frac{dT}{dz} \quad (2)$$

where q , k , T , and z , are the heat flow (W/m^2), rock thermal conductivity ($\text{W}/(\text{mK})$), temperature ($^\circ\text{C}$) and depth (m), respectively.

4. RESULTS

4.1 Subsurface rock properties and conditions

Two slimholes have been drilled to depths of 1.12 km and 1.76 km at Admiralty and Sembawang, respectively. At the surface, there is a soil layer with an approximate vertical thickness of up to 60 m. This layer includes a thin upper section of up to 6 m with a reddish-brown, mud-like texture, followed by a more substantial residual soil layer. This layer consists of gravel-sized, light grey, coarse-grained, and highly weathered rock pieces that retain the original texture of the granite. Rock coring began in earnest at the bedrock from depths of 62 m at Admiralty and 12 m at Sembawang. The dominant rock type identified past the soil layer in both locations is granite.

From the Admiralty slim hole, rock quality was found to be high in most of the slim hole (RQD >60% in Figure 7A). The granites show varying levels of alteration, as indicated by the orange-red rust-like coloring on the rocks (in Figure 7B). A dark, green-colored rock type resembling an intrusion also occurs. Mm-thick granite fractures, often filled with calcite, are common despite the high RQD values. Two weak zones with low RQD values (RQD = 0%) were observed at depths of 570 m and around 950 m. These granites are highly altered and friable upon further inspection (Figure 7C). After the first weak zone, the quality of the granite improved to RQD >80% seen in most of the rock core box (Figure 7D). Closer inspection revealed widespread hairline calcite-filled fractures highlighting multiple deformation and sealing mechanics despite high RQD values. The second weak zone is located at around 950 m to the bottom of the slim hole, where a continuous zone of highly fractured and porous granites is present (Figure 7E). This region of low rock quality was inferred as a potential fracture zone based on interpretations from previously in-house shallow soil resistivity surveys. However, the lateral extent of this zone is unknown. If the lateral extent of this zone is substantial, it could serve as a space for underground storage (e.g., CO₂ and water). Non-invasive geophysical surveys can be conducted to estimate the lateral extent of this zone.

Rock conditions in Sembawang differ significantly from those in Admiralty (Figure 8A). For the first 425 m, the rock quality is poor, with RQD values ranging from 0-40% and occurrences of fractures and varying intensities of alteration (Figure 8B). At RQD values of around 40%, the intensity of fractures in each rock core fluctuates from single fractures to localized regions of increased fracturing and alteration,

typically limited to a vertical thickness of 1 meter. At RQD of 0%, the rock texture is comparable to the rocks found at depths of 568 – 571 m at Admiralty (Figure 7C). Beyond the depth of 425 m, the rock quality generally improves with RQD values > 60%. Closer inspection reveals extensive mm-thick dark-colored mineralization that crosscuts the larger potassium feldspars. High RQD (>80%) granites are maintained at depths beyond 1,000 m. The proportion of potassium feldspars decreases significantly in favor of greyish minerals like quartz (Figure 8D). Thicker quartz veins become more common towards the end of the slim hole (Figure 8E), indicating possible hydrothermal fluid flow at depth that mechanically fractured the original granite and deposited silicate minerals.

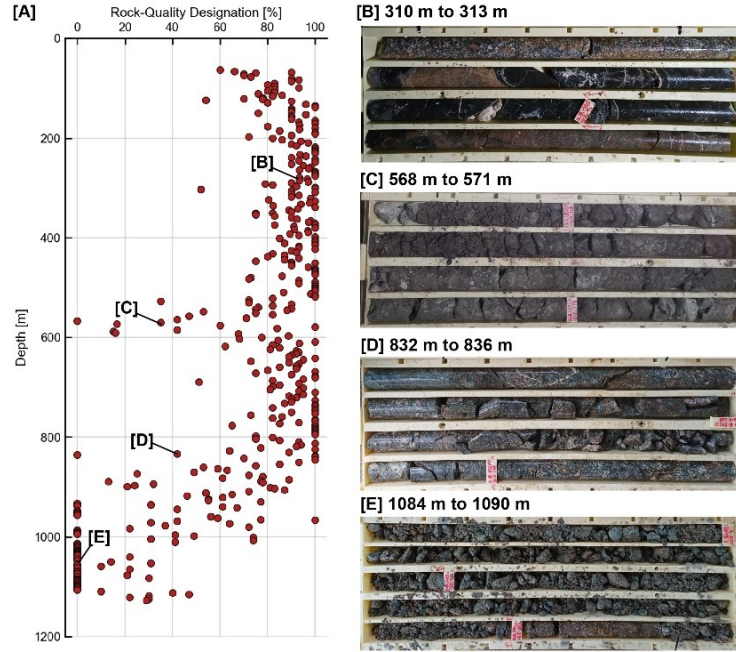


Figure 7: Rock quality designation (RQD) and selected rock core samples at Admiralty

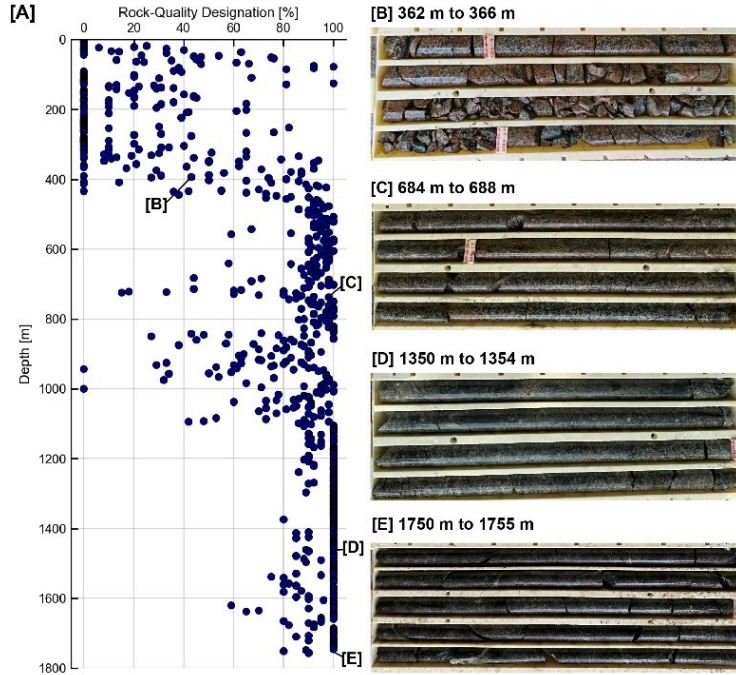


Figure 8: RQD and selected rock core samples at Sembawang

4.2 Laboratory measurements

The results and summary statistics of the laboratory measurements are shown for both slim holes in Figure 9 and Table 10.

For rock density, the distribution of the data points in both slim holes shows that most of the points reside within the range of 2.4 – 2.8 g/cm³. Apart from a few outliers found at the depths of 63 m and around 330 m for Admiralty and at 1000 m depth for Sembawang, the variance of rock core density is low at 0.01. The average density values of Admiralty and Sembawang at 2.6 and 2.7 g/cm³ are within the acceptable global range of granite density values, respectively.

Heat production values in Admiralty highlight the following trend: a maxima of heat production reaching 8 $\mu\text{W}/\text{m}^3$ at the surface, reaching a minima at around $\sim 4 \mu\text{W}/\text{m}^3$ at 450 m before increasing again to 6 $\mu\text{W}/\text{m}^3$ at 1,000 m. From the depth of 1,000 m, heat production decreased significantly to $< 1 \mu\text{W}/\text{m}^3$ due to the rock being significantly altered and weathered. The average heat production value in Admiralty is around 4.9 $\mu\text{W}/\text{m}^3$, whereas the average heat production value at Sembawang is found to be at 3.6 $\mu\text{W}/\text{m}^3$. If consistent over deeper depths (~ 10 km), the thick, high heat-producing granite can contribute significantly to Singapore's anomalously high heat flow.

Thermal conductivity values vary within the range of 2 – 4 W/(mK) and have an average of 3.3 W/(mK) for both slim holes.

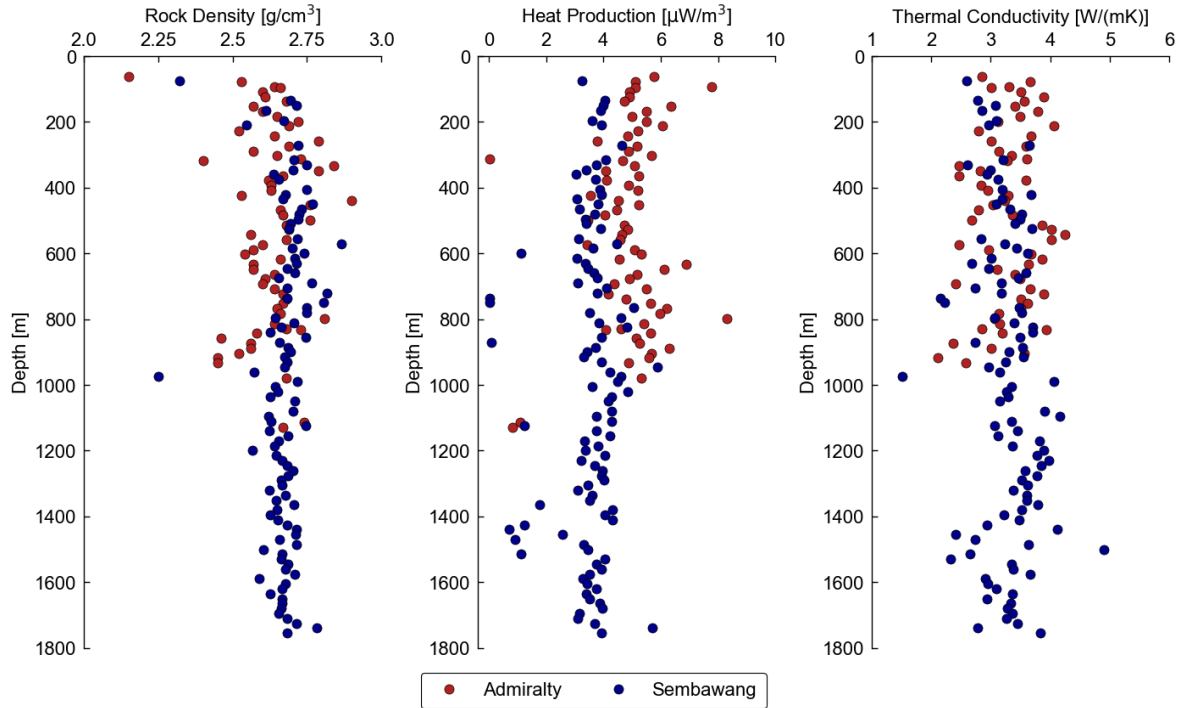


Figure 9: (From Left to Right) Measured rock density, heat production and thermal conductivity values against depth for rock core samples acquired from Admiralty (Red) and Sembawang (Blue).

Table 10: Summary statistics of the density, heat production and thermal conductivity values from Admiralty and Sembawang.

	Admiralty			Sembawang		
	Density [g/cm ³]	Heat Production [$\mu\text{W}/\text{m}^3$]	Thermal Conductivity [W/(mK)]	Density [g/cm ³]	Heat Production [$\mu\text{W}/\text{m}^3$]	Thermal Conductivity [W/(mK)]
Min	2.2	0.0	2.1	2.3	0.0	1.5
Max	2.9	8.3	4.3	2.8	5.9	4.9
Average	2.6	4.9	3.3	2.7	3.6	3.3

4.3 Temperature profile and heat flow

Figure 11 shows the measured temperature profiles for Admiralty and Sembawang with the bottom hole temperatures and depths reached are 70.5°C and 122.2°C at 1.12 km and 1.76 km, respectively. The bottom well temperature at Sembawang at 122.2°C is approaching the technical measurement limit of 125°C. An additional temperature probe with a higher temperature range (i.e., the Metrolog PTRM5) was brought in to reassess the temperature profile. Temperature values were found to be identical after multiple measurements over several

days. Additionally, the PTRM5 also measured subsurface pressure values, which were found to be consistent with theoretical hydrostatic pressure (e.g., Sibson 2020).

Both locations show a similar temperature profile at the first few hundred meters, which we refer to as the shallow subsurface. Extremely high-temperature gradients at the shallow subsurface reaching $151^{\circ}\text{C}/\text{km}$ and $93^{\circ}\text{C}/\text{km}$ for Admiralty and Sembawang, respectively.

The temperature profiles become different past the shallow subsurface. At Admiralty, the temperature gradient decreases significantly to $16^{\circ}\text{C}/\text{km}$, resulting in the temperature profile going into a sub-vertical trend between the depths of ~ 150 – 825 m. The low-temperature gradient at 150 – 825 m depth indicates a zone with convective heat transfer. Additionally, rock core samples at those depths were shown to be highly altered and weathered, which indicates the movement of hydrothermal fluids and mineralization in the subsurface (Figure 7B and C). At a depth of 825 m towards the end of the borehole, the relatively constant temperature gradient increases to $44^{\circ}\text{C}/\text{km}$ from which suggests a zone with conductive heat transfer.

For Sembawang, the temperature gradient decreased to $40^{\circ}\text{C}/\text{km}$ at depths of around 425 – 1600 m. The profile suggests that heat is mainly transferred conductively in this zone. The temperature gradient decreased again to around $9^{\circ}\text{C}/\text{km}$ after the depth of 1600 m. It remains unclear what type of temperature gradient as the drilling was halted at 1.76 km.

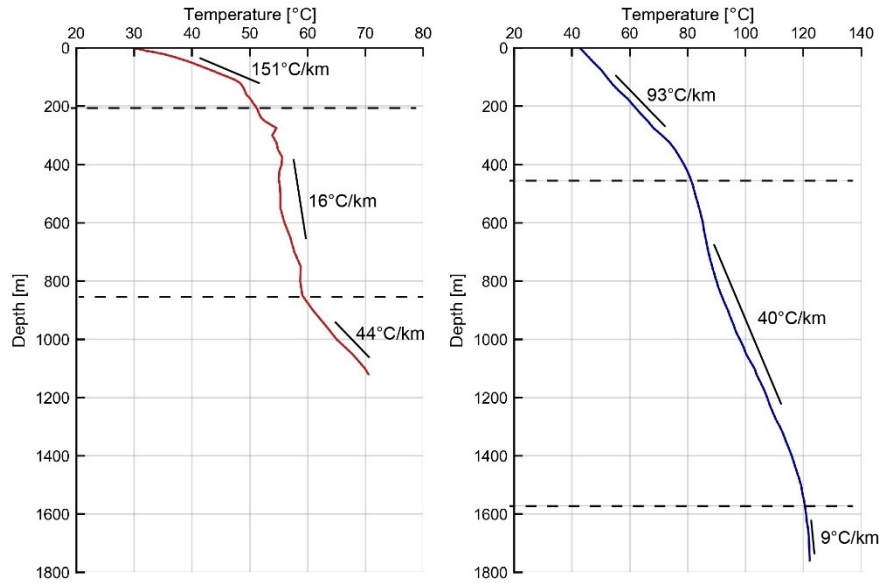


Figure 11: Measured temperature profile of Admiralty (left, red) and Sembawang (right, blue). Temperature gradients are stated in the figure.

The temperature profiles for Admiralty and Sembawang show that the thermal gradient lies between 40 – $44^{\circ}\text{C}/\text{km}$ for their conductive zones. Using the harmonic mean of rock thermal conductivity at each conductive zone ($2.8 \text{ W}/(\text{mK})$ at Admiralty and $3.3 \text{ W}/(\text{mK})$ at Sembawang, the evaluated heat flow is 125 – $131 \text{ mW}/\text{m}^2$, marking Singapore's first heat flow measurement. This range is slightly higher compared to previous estimates from regional heat flow interpolations of 110 – $130 \text{ mW}/\text{m}^2$ and thermal gradients of $37.4^{\circ}\text{C}/\text{km}$ (Hall and Morley 2004; Oliver et al. 2011).

5. DISCUSSION

5.2 Geothermal potential in Singapore

An evaluated geothermal gradient of 40 – $44^{\circ}\text{C}/\text{km}$, the surface heat flow that is twice the global average, and a granite heat production that is twice the global average indicate that there is geothermal potential in Singapore. If the geothermal gradient remains unchanged at higher depths, the rock temperatures could reach 230°C at a depth of 5 km, which is highly favorable for geothermal-powered electricity generation and direct-heat applications.

Measured temperature profiles in Singapore are hotter than other countries located in non-volcanic regions (see in Figure 12A). In Figure 12B, Bottom-well temperatures at Admiralty and Sembawang are found to be hotter compared to some deep boreholes in other non-volcanic regions such as Brühl (Germany), Basel 1 (Switzerland), Pohang BH-4 (South Korea), Lund DGE1 (Sweden), and Espoo (Finland). The wells in Soultz (France) and Landau (Germany) have one of the highest measured temperatures, and they are currently utilized as enhanced geothermal system (EGS) power plants. Additionally, the granites at Cornwall, United Kingdom, have a similar heat flow value of over $120 \text{ mW}/\text{m}^2$, and a geothermal power plant has been built and begun operations (Ledingham, Cotton, and Law 2019).

A first-order approximation of the volumetric heat capacity and power potential can be estimated. The amount of stored heat in place in Singapore within the regions of Simpang granite pluton and Tekong island (where the Unam hot spring resides as seen in Figure 1) can

be estimated by using the volumetric method. The vertical thickness of the hot rocks can be taken as 2 km (at the depth of 3 – 5 km), following Qiu et al. (2022) that described zones applicable for relatively simple practical applications.

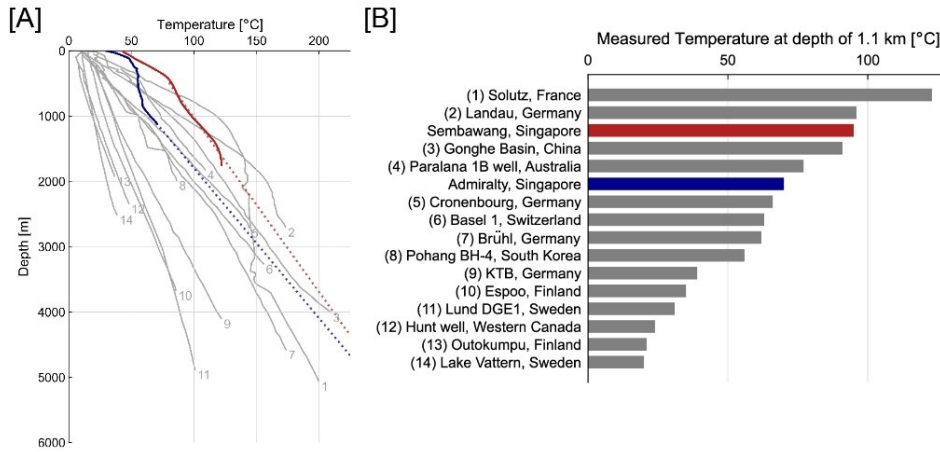


Figure 12: [A] Measured temperature profiles from Admiralty (blue) and Sembawang (red) compared against existing boreholes from other countries. The dotted blue and red lines are the linearly extrapolated profiles using measured temperatures from depth 850 m to 1100 m at Admiralty Lane slim hole and depth 1000 m to 1400 m at Gambas Avenue slim hole, respectively. **[B]** Comparison of measured temperatures at 1.1 km against deep boreholes conducted in country situated in non-volcanic regions. The grey lines are temperature profiles from boreholes around the world at locations that are not associated with volcanism: (1) Soultz GPK-2, France (Genter et al. 2010); (2) Landau, Germany (Vidal and Genter 2018); (3) Paralana 1B, Australia (Dello-Iacovo 2014); (4) Cronenbourg, Germany (Vidal and Genter 2018); (5) Brühl, Germany (Vidal and Genter 2018); (6) Basel 1, Switzerland (Ladner and Häring 2009); (7) Pohang BH-4, South Korea (Lim et al. 2020); (8) KTB, Germany (Emmermann and Lauterjung 1997); (9) Lund DGE1, Sweden (Rosberg and Erlström 2019); (10) Espoo OTN-3, Finland (I T Kukkonen and M Pentti 2020); (11) Espoo, Finland (I T Kukkonen and M Pentti 2020); (12) Hunt well, Western Canada (Majorowicz et al. 2014); (13) Lake Vattern, Sweden (Sundberg et al. 2016); (14) Outokumpu, Finland (Kukkonen et al. 2011).

Volumetric heat capacity by Brook et al. (1978), White and Williams (1975) and Ciriaco, Zarrouk, and Zakeri (2020) is expressed as:

$$q_{\text{heat}} = \rho_r c_r V (T_i - T_f) \quad (3)$$

where q_{heat} , ρ_r , c_r , V , T_i , and T_f are the heat in place (MJ), rock density (kg/m^3), rock specific heat capacity ($\text{J}/\text{kg}^{\circ}\text{C}$), the volume of rock (m^3), initial reservoir temperature and cut-off or final reservoir temperature ($^{\circ}\text{C}$), respectively.

Conversely, power potential can be estimated according to Quiniao and Zarrouk (2014) and Ciriaco, Zarrouk, and Zakeri (2020), which is expressed as

$$P = q_{\text{heat}} \frac{R_f \eta_{\text{conv}}}{FL} \quad (4)$$

where P , q_{heat} , R_f , η_{conv} , F and L are the power potential (MWe), heat-in-place (MJ), recovery factor, Organic Rankine Cycle heat-to-electricity conversion efficiency (%), load factor (%) and plant life (seconds), respectively.

Using the values listed in Table 13, the evaluated volumetric heat in place and power potential generated over 30 years is 4.2×10^{13} MJ and 810 MWe, respectively.

5.2 Techno-environmental analysis

The datasets generated from the drilling and lab measurements can be further used to ascertain geothermal utilization options for Singapore. Experimentally validated codes, such as GEOPHIRES (e.g., Beckers and McCabe 2019), *urbs* (Dorfner 2023) and an in-house MATLAB-ORC-ARC code (e.g., Schiffler et al. 2023), can simulate and estimate electricity and cooling generation, its costs from Life Cycle Assessments and Life Cycle Cost Analyses, and their corresponding potential emissions savings based on a given heat extraction technology such as EGS and Advanced Geothermal Systems (AGS). As such, a bespoke methodology has been developed to evaluate the feasibility of employing EGS and AGS for electricity and cooling generation in Singapore.

Initial results indicate that cooling and electricity generation through EGS is more competitive when compared to the Uniform Electricity Price of \$300/MWh and chilled water tariffs in Singapore. Electricity and chilled water generation using AGS are comparable to the same uniform electricity price and chilled water tariffs. Carbon emission savings, regardless of applied heat extraction technology, are significant. In tropical countries like Singapore, up to one-third of the energy used is to provide cooling (Tok et al. 2022). Chilled water can be generated by utilizing commercially viable technologies such as absorption evaporative chillers and used in existing district cooling

networks. The impact on the carbon emissions front will be significant and strongly align with Singapore's ongoing energy transition and carbon mitigation targets. A more detailed and further optimization of the techno-economic analysis will be presented in a separate publication.

Table 13: Table of values used to provide a first-order approximation of volumetric heat in place and power potential.

Equation term	Key parameters	Value
	Applied geothermal gradient	40 – 44 °C/km
C_r	Rock heat capacity	1000 J/kg/°C
ρ_r	Rock density	2650 kg/m ³
V	Volume of productive reservoir	175 km ²
T_i	Geothermal fluid production temperature	180°C
T_f	Rejection temperature	90°C
R_f	Recovery factor	15%
η_{conv}	Organic Rankine Cycle heat-to-electricity conversion efficiency	11%
F	Load factor	90%
L	Plant Life	30 years

5.3 Significance and limitations of this work

The significance of this work cannot be understated. Firstly, the drillings were conducted to ascertain the presence of an elevated subsurface temperature located near the Sembawang hot springs, indicated by previously conducted reservoir models and literature (Tjiawi, Palmer, and Oliver 2012). The evaluated heat flow values validate the presence of Singapore's geothermal potential. Secondly, the deep slimhole drillings are the first of its kind in Singapore, and the depths reached were record-breaking. Thirdly, the extracted rock cores show that the granites at both locations differ significantly and are found to be more altered and fractured than previously understood. The presence of widespread calcite-filled fractures in Admiralty and the dark-colored mineralization fractures in Sembawang highlight multiple deformation mechanics could be at play during the formation of the Simpang Granite. Lastly, results from the Admiralty slimhole spurred initiatives by the government, such as the starting of an island-wide geophysical survey and the establishment of the Future Energy Fund. Such initiatives will be crucial to improving our understanding of Singapore's deep subsurface while developing the local talent pool for further geothermal exploration work.

The work is also not without limitations. Slimhole drilling has its advantages and challenges that are well documented (e.g., Adityatama et al. 2020). These challenges include limited well measurements that can be taken such as temperature and physical rock cores. The small diameter of slimhole also restricts other measurements, including acoustic imaging, downhole geophysics and pumping tests. The slimholes in Singapore encountered zones of highly altered and weathered rocks that potentially compromised the well integrity even though casing was installed throughout the process. Additionally, the talent pool needed for geothermal exploration and drilling is highly specialized and its skillset stems from the oil and gas industry (e.g., IEA 2024a). Unlike other countries, Singapore does not have an established upstream oil and gas industry and therefore, has limited access to a local talent pool.

6. CONCLUSION

The completion of the two deep exploratory slim holes in northern Singapore represents the initial steps for geothermal exploration. Bottom hole temperatures, higher than average temperature gradients, and the presence of high heat producing rocks are found to be favorable for Singapore's geothermal potential. Initial techno and environmental analyses on using geothermal highlight significant reductions in carbon emissions – and could prove to be critical in Singapore's decarbonization efforts.

Moving forward, the proposed work will involve deep drilling as current data indicate that Singapore's geothermal system is conduction-dominated. The proposed work has two main goals: validating the temperature at 5 km depth and establishing a demonstration plant for heat extraction feasibility. A potential collaboration could involve creating a deep borehole laboratory, a concept previously implemented

by other universities like Cornell and TU Delft. Additionally, the cost for developing geothermal is projected to decrease due to its current pace of technological advancements pertaining to drilling costs that enable other countries to reach high-quality heat at deeper depths. Singapore can benefit from ongoing exploration and building local knowledge pools, positioning itself to adopt emerging technologies effectively.

7. ACKNOWLEDGEMENTS

This work is supported by the National Research Foundation under the Intra-CREATE Thematic Grant “Cities” (Grant Number: NRF2019-THE001-002).

REFERENCES

Adityatama, Daniel, Dorman Purba, Farhan Muhammad, Vicki Agustino, Hafni Wiharlan, and Kathryn K. Pasmeputra. 2020. “Slim Hole Drilling Overview for Geothermal Exploration in Indonesia: Potential and Challenges.” In *Proceedings 45th Workshop on Geothermal Reservoir Engineering*, 13. Stanford, California. <https://pangea.stanford.edu/ERE/db/GeoConf/papers/SGW/2020/Adityatama.pdf>.

Annels, A. E., and S. C. Dominy. 2003. “Core Recovery and Quality: Important Factors in Mineral Resource Estimation.” *Applied Earth Science* 112 (3): 305–12. <https://doi.org/10.1179/037174503225011306>.

Baioumy, Hassan, Mohd Nawawi, Karl Wagner, and Mohd Hariri Arifin. 2015. “Geochemistry and Geothermometry of Non-Volcanic Hot Springs in West Malaysia.” *Journal of Volcanology and Geothermal Research* 290 (January):12–22. <https://doi.org/10.1016/j.jvolgeores.2014.11.014>.

Bea, Fernando. 2012. “The Sources of Energy for Crustal Melting and the Geochemistry of Heat-Producing Elements.” *Lithos* 153 (November):278–291. <https://doi.org/10.1016/j.lithos.2012.01.017>.

Beckers, Koenraad F., and Kevin McCabe. 2019. “GEOPHIRES v2.0: Updated Geothermal Techno-Economic Simulation Tool.” *Geothermal Energy* 7 (1): 5. <https://doi.org/10.1186/s40517-019-0119-6>.

Brook, C. A., R. H. Mariner, D. R. Mabey, J. R. Swanson, Marianne Guffanti, and L. J. P. Muffler. 1978. “Hydrothermal Convection Systems with Reservoir Temperatures $\geq 90^{\circ}\text{C}$.” 790. U.S. Geological Survey. <https://doi.org/10.3133/cir790>.

Bücker, Christian, and Ladislaus Rybach. 1996. “A Simple Method to Determine Heat Production from Gamma-Ray Logs.” *Marine and Petroleum Geology* 13 (4): 373–75. [https://doi.org/10.1016/0264-8172\(95\)00089-5](https://doi.org/10.1016/0264-8172(95)00089-5).

Building and Construction Authority. 2021. “Singapore Geology (2021): Interactive 1:50 000 Scale Map.” Singapore: Building and Construction Authority. <https://form.gov.sg/6107a2b7c91529001290be54>.

Chua, Stephen, Adam D. Switzer, Timothy I. Kearsey, Michael I. Bird, Cassandra Rowe, Kiefer Chiam, and Benjamin P. Horton. 2020. “A New Quaternary Stratigraphy of the Kallang River Basin, Singapore: Implications for Urban Development and Geotechnical Engineering in Singapore.” *Journal of Asian Earth Sciences* 200 (September):104430. <https://doi.org/10.1016/j.jseas.2020.104430>.

Ciriaco, Anthony E., Sadiq J. Zarrouk, and Golbon Zakeri. 2020. “Geothermal Resource and Reserve Assessment Methodology: Overview, Analysis and Future Directions.” *Renewable and Sustainable Energy Reviews* 119 (March):31. <https://doi.org/10.1016/j.rser.2019.109515>.

Dello-Iacovo, M. 2014. “South Australian Heat Flow Anomaly: Source and Implications for Geothermal Energy.” Adelaide, Australia: University of Adelaide. <https://digital.library.adelaide.edu.au/dspace/bitstream/2440/109977/2/02wholeGeoHon.pdf>.

Dodd, Thomas J. H., Martin R. Gillespie, A. Graham Leslie, Timothy I. Kearsey, Rhian S. Kendall, Thomas P. Bide, Marcus R. Dobbs, et al. 2019. “Paleozoic to Cenozoic Sedimentary Bedrock Geology and Lithostratigraphy of Singapore.” *Journal of Asian Earth Sciences* 180 (August):103878. <https://doi.org/10.1016/j.jseas.2019.103878>.

Dodd, Thomas J. H., A. Graham Leslie, Martin R. Gillespie, Marcus R. Dobbs, Thomas P. Bide, Rhian S. Kendall, Timothy I. Kearsey, Kiefer Chiam, and Michael Goay. 2020. “Deep to Shallow-Marine Sedimentology and Impact of Volcanism within the Middle Triassic Palaeo-Tethyan Semantan Basin, Singapore.” *Journal of Asian Earth Sciences* 196 (July):104371. <https://doi.org/10.1016/j.jseas.2020.104371>.

Dorfner, Johannes. 2023. “Urbs: A Linear Optimisation Model for Distributed Energy Systems.” Python. Munich, Germany: Chair of Renewable and Sustainable Energy Systems, Technical University of Munich. <https://urbs.readthedocs.io/en/latest/>.

EMA. 2022. “Charting the Energy Transition to 2050: Energy 2050 Committee Report.” Singapore: Energy Market Authority.

Emmermann, Rolf, and Jörn Lauterjung. 1997. “The German Continental Deep Drilling Program KTB: Overview and Major Results.” *Journal of Geophysical Research: Solid Earth* 102 (B8): 18179–201. <https://doi.org/10.1029/96JB03945>.

Genter, Albert, Keith Evans, Nicolas Cuenot, Daniel Fritsch, and Bernard Sanjuan. 2010. “Contribution of the Exploration of Deep Crystalline Fractured Reservoir of Soultz to the Knowledge of Enhanced Geothermal Systems (EGS).” *Comptes Rendus Geoscience* 342 (7–8): 502–16. <https://doi.org/10.1016/j.crte.2010.01.006>.

Gillespie, Martin R., Rhian S. Kendall, A. Graham Leslie, Ian L. Millar, Thomas J.H. Dodd, Timothy I. Kearsey, Thomas P. Bide, et al. 2019. “The Igneous Rocks of Singapore: New Insights to Palaeozoic and Mesozoic Assembly of the Sukhothai Arc.” *Journal of Asian Earth Sciences* 183 (October):103940. <https://doi.org/10.1016/j.jseas.2019.103940>.

Hall, Robert, and Christopher K. Morley. 2004. “Sundaland Basins.” In *Geophysical Monograph Series*, edited by Peter Clift, Wolfgang Kuhnt, Pinxian Wang, and Dennis Hayes, 149:55–85. Washington, D. C.: American Geophysical Union. <https://doi.org/10.1029/149GM04>.

Hamza, V. M., R. R. Cardoso, and C. F. Ponte Neto. 2008. “Spherical Harmonic Analysis of Earth’s Conductive Heat Flow.” *International Journal of Earth Sciences* 97 (2): 205–26. <https://doi.org/10.1007/s00531-007-0254-3>.

I T Kukkonen, and M Pentti. 2020. “St1 Deep Heat Project: Geothermal Energy to the District Heating Network in Espoo.” In , 5. IOP Conf. Series: Earth and Environmental Science. Helsinki: IOP Publishing. <https://doi.org/10.1088/1755-1315/703/1/012035>.

IEA. 2024a. "The Future of Geothermal Energy." Paris: International Energy Agency. <https://iea.blob.core.windows.net/assets/b5b73936-ee21-4e38-843b-8ba7430fbe92/TheFutureofGeothermal.pdf>.

———. 2024b. "World Energy Investment 2024." Paris: International Energy Agency. <https://www.iea.org/reports/world-energy-investment-2024/>.

Kukkonen, Ilmo T., Volker Rath, Liisa Kivekäs, Jan Šafanda, and Vladimir Čermak. 2011. "Geothermal Studies of the Outokumpu Deep Drill Hole, Finland: Vertical Variation in Heat Flow and Palaeoclimatic Implications." *Physics of the Earth and Planetary Interiors* 188 (1–2): 9–25. <https://doi.org/10.1016/j.pepi.2011.06.002>.

Ladner, Florentin, and Markus O Häring. 2009. "Hydraulic Characteristics of the Basel 1 Enhanced Geothermal System." *GRC Transactions* 33:5.

Lazard. 2024. "Lazard LCOE+ Report 2024." Levelized Cost of Energy+. <https://www.lazard.com/research-insights/levelized-cost-of-energyplus/>.

Ledingham, Peter, Lucy Cotton, and Ryan Law. 2019. "The United Downs Deep Geothermal Power Project." In *44th Workshop on Geothermal Reservoir Engineering*, 11. Stanford, California. <https://pangea.stanford.edu/ERE/pdf/IGAstandard/SGW/2019/Law.pdf>.

Leslie, A. Graham, Thomas J. H. Dodd, Martin R. Gillespie, Rhian S. Kendall, Thomas P. Bide, Timothy I. Kearsey, Marcus R. Dobbs, Michael Kim Woon Lee, and Kiefer Chiam. 2019. "Ductile and Brittle Deformation in Singapore: A Record of Mesozoic Orogeny and Amalgamation in Sundaland, and of Post-Orogenic Faulting." *Journal of Asian Earth Sciences* 181 (September):103890. <https://doi.org/10.1016/j.jseas.2019.103890>.

Lim, Woo-Ri, Se-Yeong Hamm, Cholwoo Lee, Seho Hwang, In-Hwa Park, and Hyoung-Chan Kim. 2020. "Characteristics of Deep Groundwater Flow and Temperature in the Tertiary Pohang Area, South Korea." *Applied Sciences* 10 (15): 5120. <https://doi.org/10.3390/app10155120>.

Majorowicz, Jacek, Judith Chan, James Crowell, Will Gosnold, Larry M. Heaman, Jochem Kück, Greg Nieuwenhuis, et al. 2014. "The First Deep Heat Flow Determination in Crystalline Basement Rocks beneath the Western Canadian Sedimentary Basin." *Geophysical Journal International* 197 (2): 731–47. <https://doi.org/10.1093/gji/ggu065>.

Oliver, G. J.H., A. C. Palmer, H. Tjiawi, and F. Zulkefli. 2011. "Engineered Geothermal Power Systems for Singapore." *The IES Journal Part A: Civil & Structural Engineering* 4 (4): 245–53. <https://doi.org/10.1080/19373260.2011.598261>.

Qiu, Lihua, Li He, Yu Kang, and Dongzhe Liang. 2022. "Assessment of the Potential of Enhanced Geothermal Systems in Asia under the Impact of Global Warming." *Renewable Energy* 194 (July):636–46. <https://doi.org/10.1016/j.renene.2022.05.130>.

Quinao, Jaime Jose, and Sadiq J Zarrouk. 2014. "A Review of the Volumetric Store-Heat Resource Assessment: One Method, Different Results." In *Proceedings 36th New Zealand Geothermal Workshop*, 1–5. Auckland, New Zealand. <http://www.geothermal-energy.org/pdf/IGAstandard/NZGW/2014/70.Quinao.pdf>.

Rosberg, Jan-Erik, and Mikael Erlström. 2019. "Evaluation of the Lund Deep Geothermal Exploration Project in the Romeleåsen Fault Zone, South Sweden: A Case Study." *Geothermal Energy* 7 (1): 10. <https://doi.org/10.1186/s40517-019-0126-7>.

Santoyo, E, and L Díaz-González. 2010. "A New Improved Proposal of the Na/K Geothermometer to Estimate Deep Equilibrium Temperatures and Their Uncertainties in Geothermal Systems." In *Proceedings World Geothermal Congress 2010*, 1–9. Bali, Indonesia. <https://www.geothermal-energy.org/pdf/IGAstandard/WGC/2010/1435.pdf>.

Satman, Abdurrahman, and Omer Inanc Tureyen. 2016. "Geothermal Wellbore Heat Transmission: Stabilization Times for 'Static' and 'Transient' Wellbore Temperature Profiles." *Geothermics* 64 (November):482–89. <https://doi.org/10.1016/j.geothermics.2016.07.003>.

Schifflechner, Christopher, Lara Kuhnert, Ludwig Irrgang, Fabian Dawo, Florian Kaufmann, Christoph Wieland, and Hartmut Spleithoff. 2023. "Geothermal Trigeneration Systems with Organic Rankine Cycles: Evaluation of Different Plant Configurations Considering Part Load Behaviour." *Renewable Energy* 207 (May):218–33. <https://doi.org/10.1016/j.renene.2023.02.042>.

Sibson, Richard H. 2020. "Dual-Driven Fault Failure in the Lower Seismogenic Zone." *Bulletin of the Seismological Society of America* 110 (2): 850–62. <https://doi.org/10.1785/0120190190>.

Siringoringo, Luhut Pardamean, Benyamin Sapiie, Alfend Rudyawan, and I Gusti Bagus Eddy Sucipta. 2024. "Origin of High Heat Flow in the Back-Arc Basins of Sumatra: An Opportunity for Geothermal Energy Development." *Energy Geoscience*, January, 100289. <https://doi.org/10.1016/j.engeos.2024.100289>.

Sundberg, Jan, Jens-Ove Näslund, Lillemor Claesson Liljedahl, John Wrafter, Matt O'Regan, Martin Jakobsson, Pedro Preto, and Sven Åke Larson. 2016. "Thermal Data for Paleoclimate Calculations from Boreholes at Lake Vättern." <https://www.skb.se/publikation/2487888/P-16-03.pdf>.

Tjiawi, Hendrik, Andrew C. Palmer, and Grahame J. H. Oliver. 2012. "Natural State Modeling of Singapore Geothermal Reservoir." *Journal of Civil Engineering, Science and Technology* 3 (December):34–40. <https://doi.org/10.33736/jcest.100.2012>.

Tok, Xinying, Hadrian Vivek, Penillard Aurore, Sophie Bordat, Kalyani Basu, and Wei Yang Lee. 2022. "Decarbonising Singapore's Energy System in the Context of Cooling." Singapore: World Wide Fund for Nature Singapore. https://www.wwf.sg/wp-content/uploads/2022/06/WWF_SG_CarbonReport.pdf.

Vidal, Jeanne, and Albert Genter. 2018. "Overview of Naturally Permeable Fractured Reservoirs in the Central and Southern Upper Rhine Graben: Insights from Geothermal Wells." *Geothermics* 74 (July):57–73. <https://doi.org/10.1016/j.geothermics.2018.02.003>.

White, Donald Edward, and David L. Williams. 1975. "Assessment of Geothermal Resources of the United States, 1975." 726. U.S. Dept. of the Interior, Geological Survey., <https://pubs.er.usgs.gov/publication/cir726>.

Zhang, Qi, Yi Hu, Jianbin Jiao, and Shouyang Wang. 2024. "The Impact of Russia–Ukraine War on Crude Oil Prices: An EMC Framework." *Humanities and Social Sciences Communications* 11 (1): 1–8. <https://doi.org/10.1057/s41599-023-02526-9>.

Zhao, J., C. N. Chen, and J. G. Cai. 2002. "A Hydrogeological Study of the Sembawang Hot Spring in Singapore." *Bulletin of Engineering Geology and the Environment* 61 (1): 59–71. <https://doi.org/10.1007/s10064-001-0143-0>.